Journal of Materials Chemistry C

PAPER

View Article Online
View Journal | View Issue

Cite this: J. Mater. Chem. C, 2019, 7, 8607

Regulating the color output and simultaneously enhancing the intensity of upconversion nanoparticles *via* a dye sensitization strategy†

Bin Xue, ‡[ab] Dan Wang, ‡[a] Youlin Zhang,[b] Jing Zuo,[b] Yulei Chang,[b] Langping Tu,*[b] Xiaomin Liu,[c] Zhen Yuan,[d] Huiying Zhao,[e] Jun Song,*[a] Junle Qu*[a] and Xianggui Kong*[b]

Received 30th April 2019,
Accepted 16th June 2019

DOI: 10.1039/c9tc02293g

rsc.li/materials-c

Color-modulated upconversion nanoparticles (UCNPs) have garnered widespread optical applications owing to their superior properties, including low auto-fluorescence background noise, large anti-Stokes shift, and distinguishable sharp emission bands. Recent success in multicolor alteration of UCNPs has mostly relied on the cross-relaxation between activators and other elements, which allows them to perform excellently in optical encoding and bioimaging. However, the color modulation is subject to the cross-relaxation strategy, which heavily weakens the original emission intensity of the activators. Herein, we report a dye-sensitization strategy of conjugating strong near-infrared absorptive dyes on the surface of UCNPs. It was proven that dye sensitization can manipulate the red to green (R/G) emission ratio of $NaYF_4$:Yb/Er@$NaYF_4$:Nd UCNPs and simultaneously enhance their luminescence intensity. The R/G emission ratio can be tuned to increase or decrease, benefiting from the dye sensitization strategy. Proof of concept was demonstrated for anti-counterfeiting application under orthogonal excitation of 808 nm and 980 nm.

1. Introduction

Upconversion luminescence (UCL) generated from trivalent lanthanide ion (Ln^{3+})-doped nanoparticles have provoked much attention in biological research and biomedical applications due to the deep penetrable near-infrared (NIR) light excitation.[1–6] Together with their other unique merits including low auto-fluorescence background noise, clear emissions far-separated from the excitation wavelength, and narrow emission bands, upconversion nanoparticles (UCNPs) have advanced many applications in sensing,[7,8] displays,[9] anti-counterfeiting[10–12] and super-resolution nanoscopy.[13–16] The abundant ladder-like energy levels of Ln^{3+} provide a large space to yield different output colors. Thus, manipulating their NIR-triggered visible emissions will extremely broaden and open extensive applications of UCNPs.

Many research efforts have been devoted to the color modulation of UCL. The most classic strategy is to dope other dopants, which will tune the UC spectra through cross-relaxation with activators. For example, the activator ions of Er^{3+}, Tm^{3+}, and Ho^{3+} can usually induce cross-relaxation with each other.[17–19] The other lanthanide ions including Sm^{3+}, Pr^{3+}, Ce^{3+}, and Eu^{3+} are also regularly doped into UCNPs to tune their emissions by inducing cross-relaxations.[20–22] Recently, transition metal ions (Mn^{2+}, Ni^{2+}, and Cr^{3+}) were also introduced to induce cross-relaxation and energy transfer with lanthanide ions.[23–25] Besides the abundant cross-relaxation strategy, controlling the dopant distance[26,27] and engineering the energy migration (Yb^{3+} → Tm^{3+} → Gd^{3+} → activators)[28,29] have also been reported to generate more varieties of emissions. In addition, coating organic dyes to absorb or quench the emission bands also provide an exciting strategy to tune the UC emissions.[30] However, most strategies are based on energy transfer from the original activators, which may weaken the UCL, especially the classic cross-relaxation method. Accordingly, tuning the emissions without sacrificing the UCL intensity is challenging.

Recently, conjugating near-infrared dyes on the surface of UCNPs provided a new avenue to enhance the UCL intensity

[a] Key Laboratory of Optoelectronic Devices and Systems of Ministry of Education and Guangdong Province, College of Physics and Optoelectronic Engineering, Shenzhen University, Shenzhen 518060, P. R. China. E-mail: songjun@szu.edu.cn, jlqu@szu.edu.cn
[b] State Key Laboratory of Luminescence and Applications, Changchun Institute of Optics, Fine Mechanics and Physics, Chinese Academy of Sciences, 130033 Changchun, China. E-mail: tulangping@163.com, xgkong14@ciomp.ac.cn
[c] State Key Laboratory on Integrated Optoelectronics, College of Electronic Science and Engineering, Jilin University, Changchun 130012, People's Republic of China
[d] Bioimaging Core, Faculty of Health Sciences, University of Macau, Macao, China
[e] The First Hospital, Jilin University, Changchun 130021, P. R. China

† Electronic supplementary information (ESI) available: Supporting data, theory and analysis. See DOI: 10.1039/c9tc02293g

‡ These authors contributed equally.

and broaden the excitation range of UCNPs.[31–33] Thus, dye-sensitized UCNPs have been used for sensing,[34] information security,[35] optogenetics,[36] and theranostics.[37] Very recently, we uncovered the potential dissipative mechanism behind the dye-sensitized UCL.[38] In this work, interestingly, we reveal another new function generated by dye sensitization, namely, tuning the upconversion spectral profile of Er^{3+}. We demonstrate that the dye-sensitization strategy can precisely tune the red/green (R/G) emission ratio and simultaneously enhance the UCL intensity. The color tuning mechanism is also revealed in detail. Furthermore, we conducted a proof of concept experiment for demonstrating its potential applications in anti-counterfeiting.

2. Experimental

2.1 Materials and reagents

4-Mercaptobenzoic acid (4-MBA, 99%), IR-780 iodide (99%), erbium(III) chloride hexahydrate ($ErCl_3{\cdot}6H_2O$, 99.99%), holmium(III) chloride hexahydrate ($HoCl_3{\cdot}6H_2O$, 99.99%), cerium(III) chloride hexahydrate ($CeCl_3{\cdot}6H_2O$, 99.99%), ytterbium(III) chloride hexahydrate ($YbCl_3{\cdot}6H_2O$, 99.99%), yttrium(III) chloride hexahydrate ($YCl_3{\cdot}6H_2O$, 99.99%), neodymium(III) oxide (Nd_2O_3, 99.99%), polydimethylsiloxane (PDMS), 1-octadecene (90%) (ODE), oleylamine (OM, 90%) and oleic acid (OA, 90%) were purchased from Sigma-Aldrich. CF_3COONa, $Y(CF_3COO)_3$, and $Yb(CF_3COO)_3$, were purchased from GFS Chemicals. NaOH, NH_4F, CH_2Cl_2, and $CHCl_3$ were purchased from Beijing Chemical Works. $Nd(CF_3COO)_3$ was synthesized by dissolving Nd_2O_3 in excess CF_3COOH and then evaporating CF_3COOH and water completely. All chemical reagents were used as received without further purification.

2.2 Procedure for the synthesis of IR-806

IR-806 was synthesized according to the method described in the literature.[31,38] Firstly, 4-MBA (115.5 mg) and IR-780 iodide (250 mg) were mixed in DMF (10 mL) in a 50 mL three-neck round bottom flask. Then, the mixed solutions were kept 17 h under N_2 protection. Then, the solution was filtered with a 0.45 μm PTFE syringe filter, and distilled under reduced pressure to remove DMF. The residue was dissolved in CH_2Cl_2 (5 mL). Then the solution was filtered again through a 0.45 μm PTFE syringe filter and the final product was precipitated using cool diethyl ether. Finally, the product was collected by vacuum filtration and dried under vacuum.

2.3 General procedure for the synthesis of Nd-shell precursor

The typical synthesis of $NaYF_4$:Nd (20%) shell precursor, which was prepared following our previous report, was as follows.[39] Neodymium trifluoroacetate precursor $Nd(CF_3COO)_3$ (0.2 mmol), yttrium trifluoroacetate (0.8 mmol) and sodium trifluoroacetate (1 mmol) were added to the precursors together with 1-octadecene (5 mL) oleic acid (3 mL) and oleylamine (3 mL). Then the mixed solution was heated to 120 °C under vacuum for 45 min to remove the residual water and oxygen. The obtained transparent solution was subsequently heated to 290 °C (under argon and vigorous stirring for 45 min), and then cooled to room temperature. The resulting nanoparticles were washed with ethanol and finally dispersed in 2 mL ODE.

2.4 General procedure for the synthesis of core–shell UCNPs

The $NaYF_4$:Yb/Er (x/2%, x = 10, 20, 25)@$NaYF_4$:Nd (20%) nanoparticles, $NaYF_4$:Yb/Er (25/x%, x = 2, 5, 10, and 20)@$NaYF_4$:Nd (20%) nanoparticles and $NaYF_4$:Yb/Ho/Ce (10/2/10%)@$NaYF_4$ nanoparticles were prepared following our previous reports.[39]

2.5 Conjugating IR-806 on the surface of core–shell UCNPs

The overall conjugating process of IR-806 dye on the surface of UCNPs was similar to that in our previous reports.[38] The UCNPs were centrifuged at least three times to remove the OA ligands as much as possible. As an example, for binding with β-$NaYF_4$:Yb/Er (25/2%)@$NaYF_4$:Nd (20%) nanoparticles, 1 mL IR-806 (x mg mL^{-1}, x = 0–20 mg mL^{-1}) in $CHCl_3$ was firstly mixed with 1 mL β-$NaYF_4$:Yb/Er (25/2%)@$NaYF_4$:Nd (20%) nanoparticles (the activator concentration of Er^{3+} ~1.67 mM) in $CHCl_3$. Then, the mixture was stirred for 24 h at room temperature, centrifuged and re-dispersed in 1 mL $CHCl_3$. The estimation of the number of dye molecules per UCNP was done according to our previous report.[38] The final solution was covered with aluminum foil and stored in the dark. In addition, the IR-806-sensitized UCNP solution was diluted at least 200 times to test its luminescence.

2.6 Preparation of ink solutions for anti-counterfeiting

100 μL of as-prepared dye-sensitized $NaYF_4$:Yb/Er (25/2%)@$NaYF_4$:Nd (20%) nanoparticles (~0.5 mg mL^{-1}) and 100 μL $NaYF_4$:Yb/Ho/Ce (10/2/10%)@$NaYF_4$ nanoparticles (~20 mg mL^{-1}) were mixed with 10 μL PDMS in a plastic tube (2.0 mL). After the solutions were uniformly mixed, 5 μL of the mixed solution was pasted on paper and the pasting procedure was repeated several times to obtain the anti-counterfeiting pattern.

2.7 General sample characterization

Transmission electron microscopy (TEM) measurements were performed on a Tecnai G2 F20 S-Twin electron microscope operating at 200 kV. X-ray diffraction (XRD) measurements were performed on a Rigaku D/max-2000 diffractometer using CuKα radiation (λ = 1.5406 Å). Luminescence spectra were acquired with an FLS980 spectrometer under the excitation of an 808 nm laser. Absorption spectra were recorded on a UV-3101 spectrophotometer. The luminescence lifetimes of the UCNPs were measured with a 500 MHz TDS 3052 Tektronix digital oscilloscope and excitation light resource generated from an Optical Parametric Oscillator (Sunlite 8000).

3. Results and discussion

The core–shell nanostructures included the $NaYF_4$:Yb/Er core as the luminescence core, and Nd-doped shell as the bridge

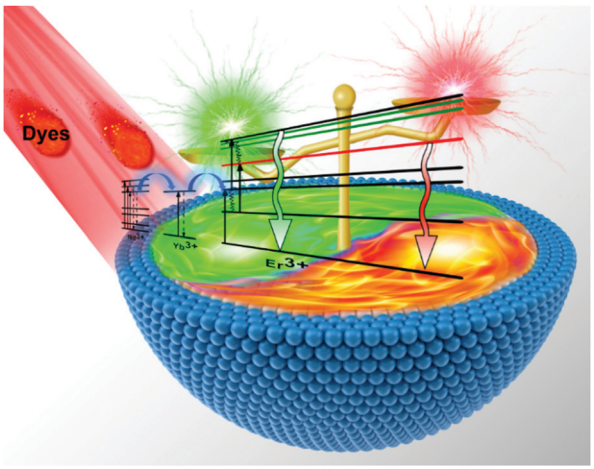

Scheme 1 Schematic diagram illustrating the dye-sensitization strategy to tune the R/G emission ratio of UCNPs.

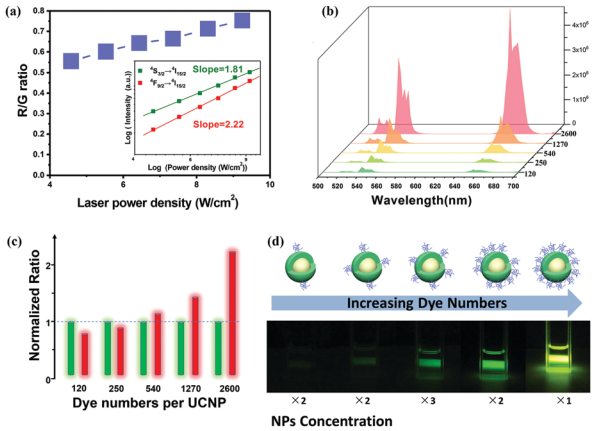

Fig. 2 (a) R/G ratio as a function of laser power density of the $NaYF_4$:Yb/Er (25/2%)@$NaYF_4$:Nd (20%) nanoparticles, and inset picture shows the log–log plots of the UCL intensity *versus* laser power density. UCL spectra (b), changed R/G emission ratio (c) and photos (d) of the dye-sensitized UCNPs with an increase in the number of conjugated dye molecules per UCNP (from 120–2600) under 808 nm excitation (8.3 W cm^{-2}).

region to draw the excitation energy from the dye and transfer it to the inner core (Scheme 1). The dye-sensitized $NaYF_4$:Yb/Er (25/2%)@$NaYF_4$:Nd (20%) core–shell nanoparticles (~31.3 nm) were successfully prepared according to our previously reported method (Fig. S1–S7, ESI†).[38] Adopting the dye-sensitization method, similar to previous reports, the UCL was enhanced (Fig. 1a) and the excitation band was broad (Fig. S8, ESI†). However, besides the remarkable enhancement in the UCL (~44 folds), we also observed that after binding ~2600 dye molecules per UCNP, the R/G emission ratio was significantly increased (Fig. 1a). We firstly inferred that the changed R/G ratio may arise from the energy back transfer of the visible emissions from Er^{3+} ions to the dye. However, the absorption of IR-806 was very weak in the range of 500 to 700 nm (Fig. S9, ESI†), and the test solution was nearly transparent. The absorption value of the dye at 650 nm was about 8 times higher than that at 540 nm, which will lower the R/G emission ratio. However, we experimentally observed an increase in the R/G emission ratio in Fig. 1a, which indicates that the absorption of the dye at 540 or 540 nm has no influence on the R/G emission ratio. More importantly, the lifetime of green emission and red emission of Er^{3+} (Fig. 1b and c, respectively) was unchanged when different numbers of dye molecules were conjugated per UCNP, which confirmed that the energy transfer from Er^{3+} to IR-806 did not occur in the range of 500 to 700 nm. It should be noted that the longer rise time in Fig. 1b and c resulted from the energy migration process occurring in the Nd^{3+}-sensitized core–shell UCNPs.[12] Considering that the role of dye sensitization is to increase the excitation state population of UCNPs, we inferred that the variation in the R/G ratio came from the changed population process of the green ($^2H_{11/2}$/$^4S_{3/2}$) and red emission state ($^4F_{9/2}$).

In essence, the dye-sensitization method to increase the UCL intensity involves amplifying the population rates of UCNPs. This can be verified by the enhanced UCL and enhanced emission of Yb^{3+} after dye-sensitization (Fig. S10, ESI†). Traditionally, the population rates of UCNPs can be enhanced by increasing the laser power density. Fig. 2a displays the double logarithm plot generated using UCL intensity *versus* pump power density, where the UCL intensity increased with the power density. The slope values of n for the $^4S_{13/2} \rightarrow {}^4I_{15/2}$ (540 nm) and $^4F_{9/2} \rightarrow {}^4I_{15/2}$ (655 nm) transitions of the Er^{3+} ions

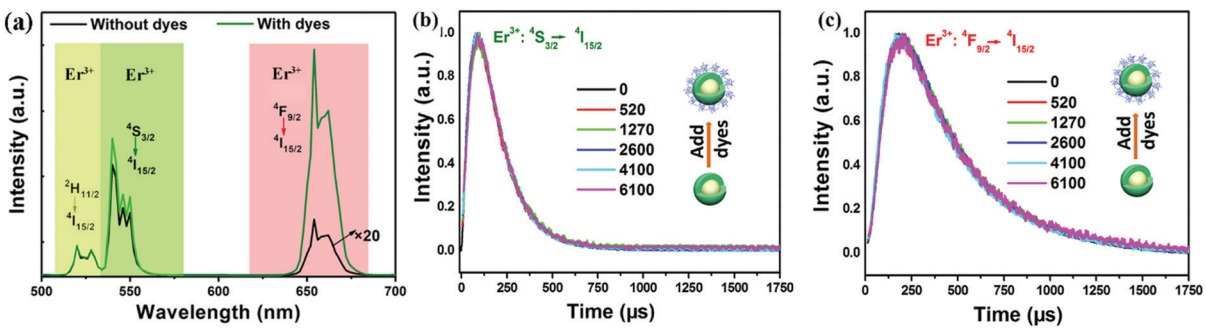

Fig. 1 (a) UCL spectra of $NaYF_4$:Yb/Er (25/2%)@$NaYF_4$:Nd (20%) nanoparticles without and with dye sensitization under excitation of 808 nm (8.3 W cm^{-2}). Luminescence decay curves of 540 nm (b) and 650 nm (c) of Er^{3+} when UCNPs conjugated with 0 (black line), 520 (red line), 1270 (green line), 2600 (blue line), 4100 (cyan line), 6100 (magenta line) dye molecules per UCNP at an excitation wavelength of 808 nm.

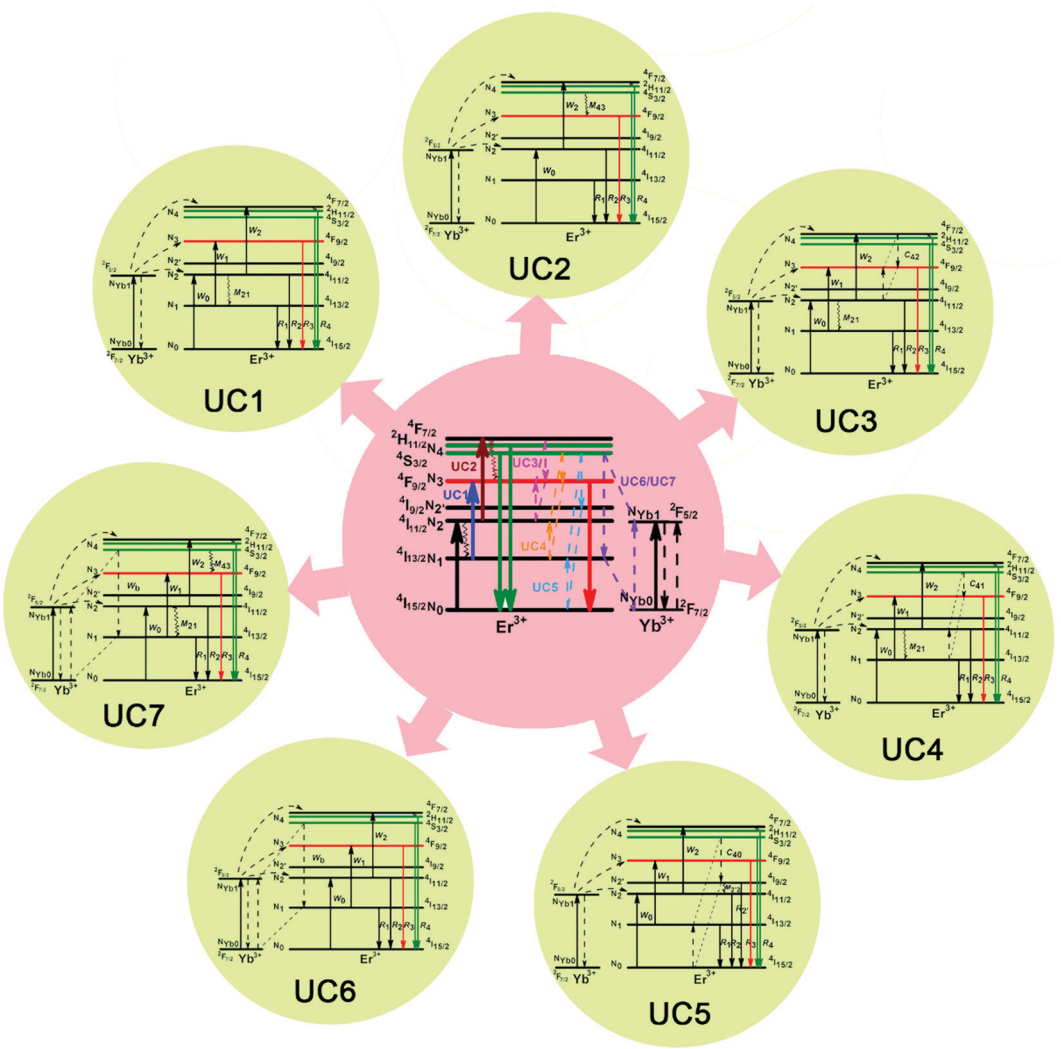

Fig. 3 Classified upconversion population scheme of the green and red emission states in the Yb^{3+}–Er^{3+} doping system. The detailed description of the UC1–UC7 process can be found in the ESI.†

were 1.81 and 2.22, respectively, characteristically indicating that multi-photon processes were involved in the green and red UC emissions. Since the slope of the red emission was larger than that of the green emission, the R/G emission ratio increased with an increase in the power density. Since dye sensitization has a similar role of increasing the power density to increase the population rates, the R/G emission ratio should also increase with an increase in the number of conjugated dye molecules per UCNP. Similarly, we mimicked the process of increased power density by increasing the number of conjugated dye molecules on the surface of the UCNPs. The UCL of the UCNPs gradually increased (Fig. 2b) after conjugating an increased number of dye molecules per UCNP (from about 120 to 2600). Initially, the R/G emission ratio was only 0.78. With a further increase in the number of conjugated dye molecules from 250 to 2600, the R/G emission ratio gradually increased (Fig. 2b–d). Finally, the red emission became dominant compared to the green emission, and the R/G emission ratio increased to 2.3. Since the population rates could be amplified by dye-sensitization (Fig. 1a), the slope difference of red/green emission on the R/G emission ratio was also remarkably amplified. Therefore, dye-sensitization can tune the R/G emission ratio according to the population difference of power-dependent R/G emission ratios. Although the dye-sensitization strategy is similar to the power-mode method, which tunes the excitation power to change the output colour, the excitation power of the laser is usually limited in a fixed range. More importantly, due to the low quantum yield of UCL, the power-mode method can induce severe overheating under a high excitation power. Differently, the dye-sensitization strategy can precisely tune the R/G emission ratio in a large range only by controlling the dye numbers per UCNP and simultaneously adopt a low excitation power due to the enhanced UCL, which is more useful for practical applications.

Apparently, deeply understanding the relationship between the R/G emission ratio and population rates will help to tune the R/G emission ratio by dye sensitization. Thus, we considered the overall UCL processes to clarify the population-dependent

Table 1 Power-dependent R/G ratio of the different upconversion processes

Upconversion mechanism	UC1	UC2	UC3	UC4	UC5	UC6	UC7
Power dependent R/G	$(a\rho + c)^{-1}$	ρ^0	ρ^0	$(\rho - c)^{-1}$	ρ^0	ρ^0	$a\rho + b$

green and red emission. The green emission, as shown in Fig. 3, is attributed to the successive energy transfer steps from Yb^{3+} to Er^{3+}, $^2F_{5/2}$ (Yb) + $^4I_{15/2}$ (Er) → $^2F_{7/2}$ (Yb) + $^4I_{11/2}$ (Er), and $^2F_{5/2}$ (Yb) + $^4I_{11/2}$ (Er) → $^2F_{7/2}$ (Yb) + $^4F_{7/2}$ (Er)[40] and the subsequent relaxation to the $^2H_{11/2}/^4S_{3/2}$ state to generate a ~525/540 nm emission. For the complex red emission of Er^{3+}, according to previous reports, the population of the $^4F_{9/2}$ state can be summarized in Fig. 3:[41–46] (i) two standard upconversion (UC) models, namely, direct population from the $^4I_{13/2}$ to $^4F_{9/2}$ state after relaxing from the $^4I_{11/2}$ to $^4I_{13/2}$ state (UC1) and relaxing from the $^2H_{11/2}/^4S_{3/2}$ state to the $^4F_{9/2}$ state (UC2); (ii) three Er–Er cross relaxation (CR) process, $^4F_{7/2}$ (Er) + $^4I_{11/2}$ (Er) → $^4F_{9/2}$ (Er) + $^4F_{9/2}$ (Er) (UC3), $^4S_{3/2}$ (Er) + $^4I_{13/2}$ (Er) → $^4F_{9/2}$ (Er) + $^4I_{11/2}$ (Er) (UC4), and $^4S_{3/2}$ (Er) + $^4I_{15/2}$ (Er) → $^4F_{9/2}$ (Er) + $^4I_{13/2}$ (Er), and subsequent ETU $^4I_{13/2}$ (Er) + $^2F_{5/2}$ (Yb) → $^4F_{9/2}$ (Er) + $^2F_{7/2}$ (Yb) (UC5); (iii) the energy transfer (EBT) from Er^{3+} to Yb^{3+}, $^4S_{3/2}$ (Er) + $^2F_{7/2}$ (Yb) → $^4I_{13/2}$ (Er) + $^2F_{5/2}$ (Yb), and then $^4I_{13/2}$ (Er) + $^2F_{5/2}$ (Yb) → $^4F_{9/2}$ (Er) $^2F_{7/2}$ (Yb), when the UC process is the dominant depletion of the $^4I_{13/2}$ state (UC6) or when linear decay is the dominant depletion of the $^4I_{13/2}$ state (UC7).[45] Since the blue UC emission was barely observable in our system, the influence from the blue UC emission state ($^2H_{9/2}$) on the green or red emission states[46] is excluded in our system. To validate the R/G emission ratio relationship, theoretical models were established and solved for the UC1–UC7 processes based on steady-state rate equations (details in the ESI†). The power-dependent R/G emission ratios of the different UC processes are listed in Table 1 (details in Table S1, ESI†). As can be seen in Table 1, only the UC1, UC4 (CR between Er^{3+} and Er^{3+}) and UC7 (EBT from Er^{3+} to Yb^{3+}) processes affected the R/G emission ratio by the power density (ρ).

Simultaneously, to further explore how the dye sensitization influenced the R/G emission ratio of the Yb/Er-doped nanosystem, we also prepared a series of UCNPs with different concentrations of Yb^{3+} ions or Er^{3+} ions in the core. Fig. 4 shows that these nanostructures with different doping concentrations of Yb^{3+} and Er^{3+} also maintained a similar size (Fig. S11, ESI†). It should be noted that the doping concentration of Yb^{3+} in the core beyond 25% resulted in the core size becoming bigger (Fig. S12 and S13, ESI†) due to the rapid growth of the crystal.[47] Therefore, we only kept the doping concentration of Yb^{3+} up to 25%.

For the $NaYF_4$:Yb/Er (25/2%)@$NaYF_4$:Nd (20%) nanoparticles, the doping concentration of Yb^{3+} was evidently larger than that of Er^{3+}; thus, the Er–Yb distance was evidently shorter than the Er–Er distance, which resulted in a more efficient EBT process from Er^{3+} to Yb^{3+} than the Er–Er CR process. Thus, the UC7 process was the most dominant process for red UC emission. According to Table 1, for the UC7 process, the R/G emission ratio increased with excitation power. Therefore, dye sensitization (similar role of increasing excitation power) increased the R/G emission ratio of the $NaYF_4$:Yb/Er (25/2%)@$NaYF_4$:Nd (20%) nanoparticles (Fig. 1a). Similarly, for the samples with ~10% Yb^{3+} and ~20% Yb^{3+} doping, the concentration of Yb was also higher than that of Er (~2%). Therefore, the UC7 process was also the dominant process in their UCL, which resulted in an increase in the R/G emission ratio with excitation power density (Fig. 5a and d). Accordingly, similarly to the samples of ~25% Yb^{3+} doping (Fig. 1a), after dye sensitization, the R/G emission ratio also increased for the samples with ~10% Yb^{3+} and ~20% Yb^{3+} doping, respectively (Fig. 5b, c, e and f, respectively). Therefore, the R/G emission ratio increased for the highly Yb-doped nanosystem after dye sensitization.

We next explored the influence of dye sensitization when doping different Er^{3+} ions. As shown in Fig. 6, besides the enhanced UCL intensity, the R/G emission ratio was evidently changed after dye sensitization. Initially, when the concentration of Er^{3+} was low (~5%) and the concentration of Yb^{3+} was high, the EBT process from Er to Yb (UC7 process) was also the dominant process because the Er–Er CR process was also weak. Similarly to the previous sample (~2% Er^{3+}, Fig. 1a), after dye-sensitization, the R/G emission ratio increased (Fig. 6a–c).

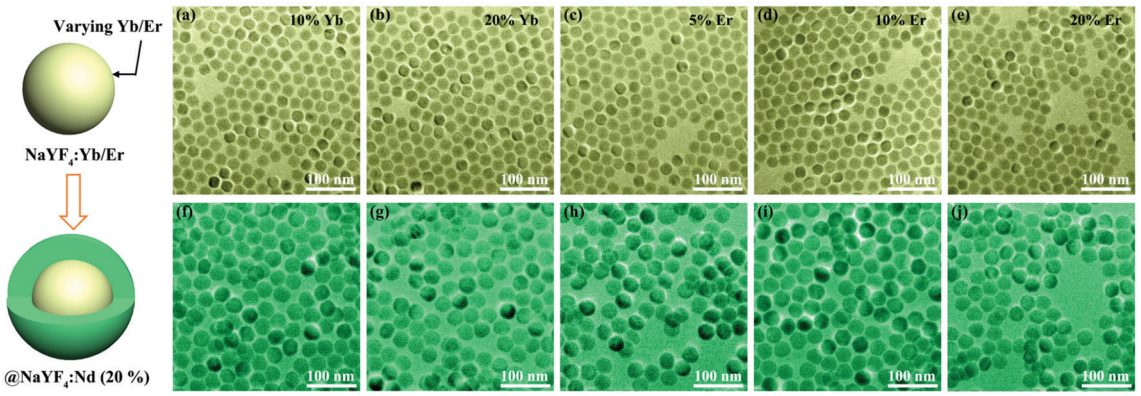

Fig. 4 TEM images of core nanoparticles of $NaYF_4$:Yb/Er (*x*/2%) nanoparticles where *x*= 10 and 20 in (a and b), and $NaYF_4$:Yb/Er (25/*x*%) nanoparticles, where *x* = 5, 10, and 20 in (c, d and e), respectively. TEM images of the corresponding core–shell nanoparticles (f–j) after coating $NaYF_4$:Nd (20%) shell corresponding to the core nanoparticles in (a–e).

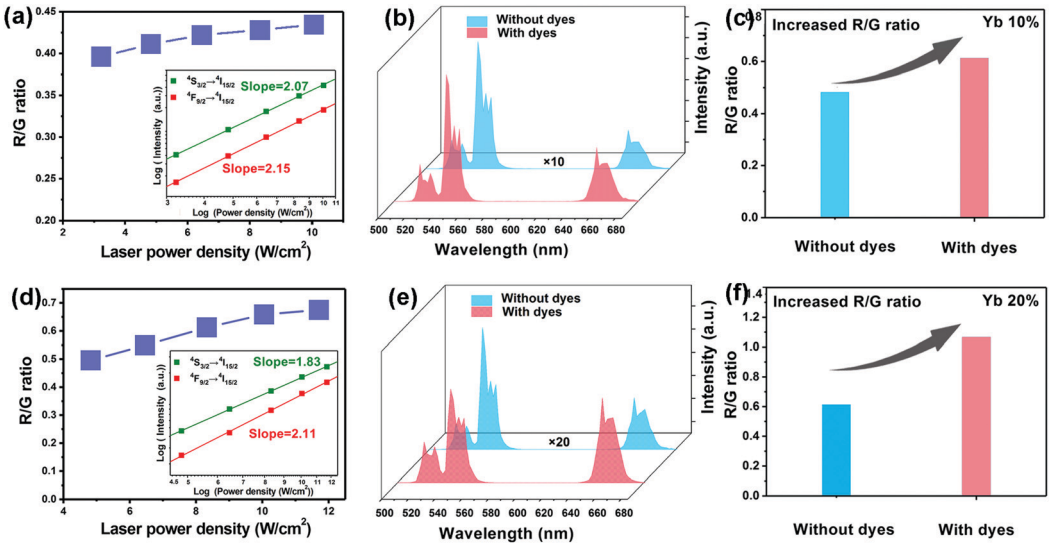

Fig. 5 R/G ratio as a function of laser power density of the $NaYF_4$:Yb/Er (10/2%)@$NaYF_4$:Nd (20%) nanoparticles (a) and $NaYF_4$:Yb/Er (20/2%)@$NaYF_4$:Nd (20%) nanoparticles (d), and inset picture shows the log–log plots of the UCL intensity *versus* laser power density. UCL spectra of $NaYF_4$:Yb/Er (10/2%)@$NaYF_4$:Nd (20%) nanoparticles (b) and $NaYF_4$:Yb/Er (20/2%)@$NaYF_4$:Nd (20%) nanoparticles (e) without or with dye sensitization under excitation of 808 nm (8.3 W cm^{-2}). The changed R/G ratio of $NaYF_4$:Yb/Er (10/2%)@$NaYF_4$:Nd (20%) nanoparticles (c) and $NaYF_4$:Yb/Er (20/2%)@$NaYF_4$:Nd (20%) nanoparticles (f) by dye sensitization.

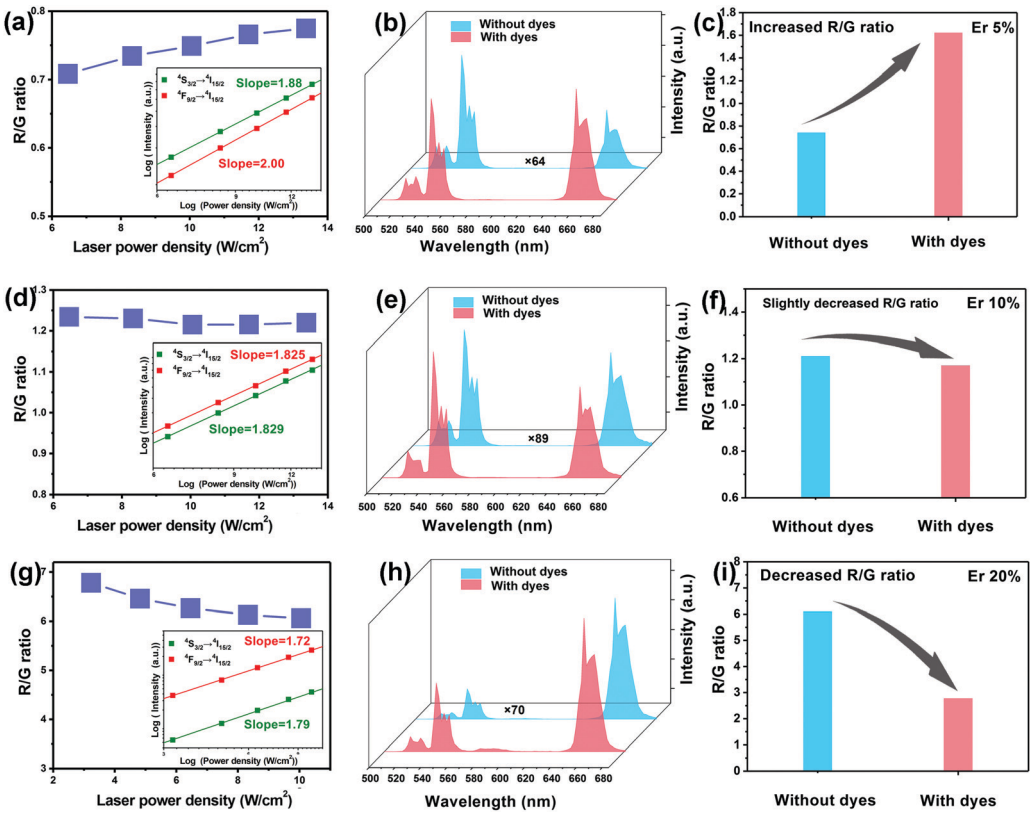

Fig. 6 R/G emission ratio as a function of laser power density of the $NaYF_4$:Yb/Er (25/5%)@$NaYF_4$:Nd (20%) nanoparticles (a), $NaYF_4$:Yb/Er (25/10%)@$NaYF_4$:Nd (20%) nanoparticles (d), and $NaYF_4$:Yb/Er (25/20%)@$NaYF_4$:Nd (20%) nanoparticles (g), inset picture shows the log–log plots of the UCL intensity *versus* laser power density; UCL spectra of $NaYF_4$:Yb/Er (25/5%)@$NaYF_4$:Nd (20%) nanoparticles (b), $NaYF_4$:Yb/Er (25/10%)@$NaYF_4$:Nd (20%) nanoparticles (e), and $NaYF_4$:Yb/Er (25/20%)@$NaYF_4$:Nd (20%) nanoparticles (h) without or with dye sensitization under an excitation of 808 nm (8.3 W cm^{-2}); the changed R/G ratio of $NaYF_4$:Yb/Er (25/5%)@$NaYF_4$:Nd (20%) nanoparticles (c), $NaYF_4$:Yb/Er (25/10%)@$NaYF_4$:Nd (20%) nanoparticles (f), and $NaYF_4$:Yb/Er (25/20%)@$NaYF_4$:Nd (20%) nanoparticles (i) by dye-sensitization.

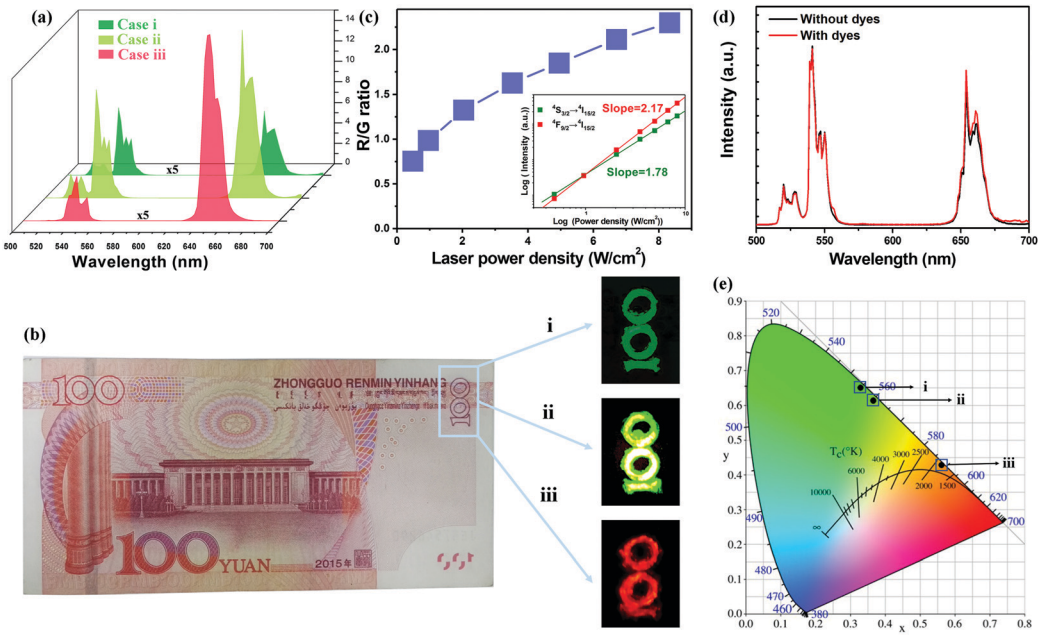

Fig. 7 (a) UCL spectra of the anti-counterfeiting ink solutions in case i (808 nm excitation, 1 W cm^{-2}), case ii (808 nm excitation, 3.5 W cm^{-2}), and case iii (980 nm excitation, 1 W cm^{-2}). (b) Anti-counterfeiting photographs of case i, case ii, and case iii. (c) R/G emission ratio as a function of laser power density of Dye-NPs, (d) UCL spectra of $NaYF_4$:Yb/Er (25/2%)@$NaYF_4$:Nd (20%) nanoparticles without and with dye sensitization under excitation of 980 nm. (e) CIE chromaticity diagram of cases i, ii, and iii.

However, when the Er^{3+} concentration gradually increased from ~5% to ~20%, apparently, the Er–Er CR process (UC4) became more and more dominant. Therefore, the dominant process changed from the UC7 process to the UC4 process. According to Table 1, the R/G emission ratio should change from increased to decreased with the excitation power, which agrees well with experimental results (Fig. 6a, d and g). Accordingly, after dye-sensitization, the R/G emission ratio changed from increased to decreased when the Er^{3+} concentration gradually increased from ~5% to ~20% (Fig. 6b, c, e, f, h and i). Therefore, the R/G emission ratio will be decreased for a highly Er-doped nanosystem or increased for a highly Er-doped nanosystem after dye sensitization (Fig. 5, 6 and Fig. S14–S16, ESI†). Taken together, all these results indicate that dye sensitization can either increase or decrease the R/G emission ratio according to the different dominant UCL population processes (UC4 and UC7 process), which highlights a new method for tuning the upconversion spectral profile.

Utilizing the unique properties (tuning the R/G emission ratio and enhancing the UCL) obtained by dye-sensitization, as a proof of concept, we designed an anti-counterfeiting application (Fig. 7a and b) based on these dye-sensitized nanostructures. The anti-counterfeiting materials were composed of the dye-sensitized $NaYF_4$:Yb/Er (25/2%)@$NaYF_4$:Nd (20%) nanoparticles (Dye-NPs) and $NaYF_4$:Yb/Ho/Ce (10/2/10%)@$NaYF_4$ nanoparticles (Ho-NPs) (Fig. S17, ESI†). On the one hand, as shown in Fig. 7a and b, under excitation of 808 nm, the emissions mainly came from the Dye-NPs because the Ho-NPs could not be excited by 808 nm light (Fig. S18, ESI†). For case (i) (power density ~1 W cm^{-2}), the green emissions were dominant compared to the red emissions. Upon increasing the power density to ~3.5 W cm^{-2} (case (ii)), the R/G emission ratio increased, which displayed a similar yellow green light. The increased R/G emission ratio arose from the amplified population ability of dye sensitization, which resulted in a larger change in the R/G emission ratio (Fig. 7c) than that of the UCNPs without dye (Fig. 2a) in the similar excitation power range. On the other hand, under 980 nm excitation, conjugating dyes with the UCNPs could not enhance the UCL (Fig. 7d), which is because the IR-806 dye has nearly no absorption at 980 nm and the Nd-doped shell could also hinder the dyes from sensitizing Yb^{3+} in the core. Therefore, when the Dye-NPs and Ho-NPs were mixed at a mass ratio of 1 : 40, the low concentration of Dye-NPs hardly interfered with the emissions of Ho-NPs (Fig. S19, ESI†), and thereby only show a distinct red emission, as shown in Fig. 7b. Moreover, according to the Commission Internationale de L'Eclairage (CIE) chromaticity diagram (Fig. 7e), the UC emissions could be tuned in a large region, especially in the eye-sensitive red and green emission region. Therefore, as shown in Fig. 7b, the orthogonal anti-counterfeiting application based on red emission and green emission under near-infrared light excitation was realized based on these unique dye-sensitized upconversion nanostructures. Traditionally, blue emission and red emission[48] or blue emission and green emission[49] can be fulfilled under orthogonal excitation of 980 nm and 808 nm, respectively. Here, based on the unique properties of dye sensitization, the eye-sensitive red light and green light anti-counterfeiting pattern was observed under orthogonal excitation of 980 nm and 808 nm, respectively.

4. Conclusions

In conclusion, we tuned the R/G emission ratio of UCNPs by dye sensitization without sacrificing the UCL intensity (even enhanced several ten times). The tuned R/G emission ratio was essentially derived from manipulating the population process of red emission and green emission of Er^{3+}. We demonstrated that the R/G emission ratio can be precisely tuned by conjugating different number of dye molecules per UCNP. Through dye sensitization, the R/G emission ratio could be increased for highly Yb-doped UCNPs or decreased for highly Er-doped UCNPs. We also summarized and solved the rate equations for the population-dependent green and red emissions, which shed light on the design of nanosystems to tune the R/G emission ratio by affecting the population process (not limited to dye-sensitization strategy). As a proof of concept, an orthogonal excited (980 nm and 808 nm) anti-counterfeiting application based on the eye-sensitive green emission and red emission was firstly fulfilled. Since this dye-sensitization strategy is still being developed, adopting dyes with more powerful amplification ability can further tune the upconversion spectral profile. Apparently, the dye-sensitization strategy essentially manipulates the upconversion spectral profile by promoting the population process of UCNPs, which can be easily extended to other activators to tune different color outputs.

Conflicts of interest

The authors declare no competing financial interest.

Acknowledgements

This work has been partially supported by the National Key R&D Program of China (2018YFC0910602); the National Natural Science Foundation of China (61775145, 11604331, 61605130, 61525503, 61620106016, 61835009, 81727804, 61575194, 11874354, 11874355, 51772122, 61875191 and 11674316); China Postdoctoral Science Foundation (2018M643143, 2018M643163). (Key)Project of Department of Education of Guangdong Province (2015KGJHZ002, 2016KCXTD007); Guangdong Natural Science Foundation Innovation Team (2014A030312008); and Shenzhen Basic Research Project (JCYJ20170412110212234, JCYJ20160328144746940, JCYJ20170412 105003520, JCYJ20180305125425815). This work was also partially supported by the University of Macau (MYRG2016-00110-FHS and MYRG2018-00081-FHS), and the Macao Science and Technology Development Fund (FDCT 025/2015/A1 and FDCT 0011/2018/A1). Project of Science and Technology Agency, Jilin Province (20180101222JC).

References

1 X. J. Zhu, Q. Q. Su, W. Feng and F. Y. Li, *Chem. Soc. Rev.*, 2017, **46**, 1025–1039.
2 F. Wang, S. Wen, H. He, B. Wang, Z. Zhou, O. Shimoni and D. Jin, *Light: Sci. Appl.*, 2018, **7**, e18007.
3 D. Wang, B. Xue, J. Song and J. L. Qu, *J. Mater. Chem. C*, 2018, **6**, 6597–6604.
4 Q. S. Wu, B. R. Huang, X. Y. Peng, S. L. He and Q. Q. Zhan, *Opt. Express*, 2017, **25**, 30885–30894.
5 B. R. Huang, Q. S. Wu, X. Y. Peng, L. Q. Yao, D. F. Peng and Q. Q. Zhan, *Nanoscale*, 2018, **10**, 21025–21030.
6 Q. Q. Zhan, J. Qian, H. J. Liang, G. Somesfalean, D. Wang, S. L. He, Z. G. Zhang and S. Andersson-Engels, *ACS Nano*, 2011, **5**, 3744–3757.
7 K. C. Liu, Z. Y. Zhang, C. X. Shan, Z. Q. Feng, J. S. Li, C. L. Song, Y. N. Bao, X. H. Qi and B. Dong, *Light: Sci. Appl.*, 2016, **5**, e16136.
8 F. Huang, T. Yang, S. X. Wang, L. Lin, T. Hu and D. Q. Chen, *J. Mater. Chem. C*, 2018, **6**, 12364–12370.
9 Z. P. Meng, S. L. Wu and S. F. Zhang, *J. Mater. Chem. C*, 2018, **6**, 13101–13107.
10 L. Lei, J. A. Xia, Y. Cheng, Y. S. Wang, G. X. Bai, H. Xia and S. Q. Xu, *J. Mater. Chem. C*, 2018, **6**, 11587–11592.
11 J. Zuo, Q. Q. Li, B. Xue, C. X. Li, Y. L. Chang, Y. L. Zhang, X. M. Liu, L. P. Tu, H. Zhang and X. G. Kong, *Nanoscale*, 2017, **9**, 7941–7946.
12 J. Zuo, D. P. Sun, L. P. Tu, Y. N. Wu, Y. H. Cao, B. Xue, Y. L. Zhang, Y. L. Chang, X. M. Liu, X. G. Kong, W. J. Buma, E. J. Meijer and H. Zhang, *Angew. Chem., Int. Ed.*, 2018, **57**, 3054–3058.
13 Y. J. Liu, Y. Q. Lu, X. S. Yang, X. L. Zheng, S. H. Wen, F. Wang, X. Vidal, J. B. Zhao, D. M. Liu, Z. G. Zhou, C. S. Ma, J. J. Zhou, J. A. Piper, P. Xi and D. Y. Jin, *Nature*, 2017, **543**, 229–233.
14 Q. Q. Zhan, H. C. Liu, B. J. Wang, Q. S. Wu, R. Pu, C. Zhou, B. R. Huang, X. Y. Peng, H. Gren and S. L. He, *Nat. Commun.*, 2017, **8**, 11.
15 R. T. Wu, Q. Q. Zhan, H. C. Liu, X. Y. Wen, B. J. Wang and S. L. He, *Opt. Express*, 2015, **23**, 32401–32412.
16 X. Y. Peng, B. R. Huang, R. Pu, H. C. Liu, T. Zhang, J. Widengren, Q. Q. Zhan and H. Agren, *Nanoscale*, 2019, **11**, 1563–1569.
17 F. Wang and X. G. Liu, *J. Am. Chem. Soc.*, 2008, **130**, 5642–5643.
18 M. Wang, C. C. Mi, Y. X. Zhang, J. L. Liu, F. Li, C. B. Mao and S. K. Xu, *J. Phys. Chem. C*, 2009, **113**, 19021–19027.
19 F. Zhang, Q. H. Shi, Y. C. Zhang, Y. F. Shi, K. L. Ding, D. Y. Zhao and G. D. Stucky, *Adv. Mater.*, 2011, **23**, 3775–3779.
20 E. M. Chan, G. Han, J. D. Goldberg, D. J. Gargas, A. D. Ostrowski, P. J. Schuck, B. E. Cohen and D. J. Milliron, *Nano Lett.*, 2012, **12**, 3839–3845.
21 G. Y. Chen, H. C. Liu, G. Somesfalean, H. J. Liang and Z. G. Zhang, *Nanotechnology*, 2009, **20**, 6.
22 D. Q. Chen, L. Liu, P. Huang, M. Y. Ding, J. S. Zhong and Z. G. Ji, *J. Phys. Chem. Lett.*, 2015, **6**, 2833–2840.
23 J. Wang, F. Wang, C. Wang, Z. Liu and X. G. Liu, *Angew. Chem., Int. Ed.*, 2011, **50**, 10369–10372.
24 Z. G. Gao, S. Guo, X. S. Lu, J. Orava, T. Wagner, L. R. Zheng, Y. Y. Liu, S. Y. Sun, F. He, P. P. Yang, J. Ren and J. Yang, *Adv. Opt. Mater.*, 2018, **6**, 9.

25 S. Ye, E. H. Song and Q. Y. Zhang, *Adv. Sci.*, 2016, **3**, 25.
26 K. Huang, N. M. Idris and Y. Zhang, *Small*, 2016, **12**, 836–852.
27 H. Dong, L. D. Sun and C. H. Yan, *Chem. Soc. Rev.*, 2015, **44**, 1608–1634.
28 F. Wang, R. R. Deng, J. Wang, Q. X. Wang, Y. Han, H. M. Zhu, X. Y. Chen and X. G. Liu, *Nat. Mater.*, 2011, **10**, 968–973.
29 L. P. Tu, X. M. Liu, F. Wu and H. Zhang, *Chem. Soc. Rev.*, 2015, **44**, 1331–1345.
30 L. Zhou, R. Wang, C. Yao, X. M. Li, C. L. Wang, X. Y. Zhang, C. J. Xu, A. J. Zeng, D. Y. Zhao and F. Zhang, *Nat. Commun.*, 2015, **6**, 10.
31 W. Q. Zou, C. Visser, J. A. Maduro, M. S. Pshenichnikov and J. C. Hummelen, *Nat. Photonics*, 2012, **6**, 560–564.
32 G. Y. Chen, J. Damasco, H. L. Qiu, W. Shao, T. Y. Ohulchanskyy, R. R. Valiev, X. Wu, G. Han, Y. Wang, C. H. Yang, H. Agren and P. N. Prasad, *Nano Lett.*, 2015, **15**, 7400–7407.
33 D. J. Garfield, N. J. Borys, S. M. Hamed, N. A. Torquato, C. A. Tajon, B. Tian, B. Shevitski, E. S. Barnard, Y. D. Suh, S. Aloni, J. B. Neaton, E. M. Chan, B. E. Cohen and P. J. Schuck, *Nat. Photonics*, 2018, **12**, 402–407.
34 X. M. Zou, X. B. Zhou, C. Cao, W. Y. Lu, W. Yuan, Q. Y. Liu, W. Feng and F. Y. Li, *Nanoscale*, 2019, **11**, 2959–2965.
35 J. Lee, B. Yoo, H. Lee, G. D. Cha, H. S. Lee, Y. Cho, S. Y. Kim, H. Seo, W. Lee, D. Son, M. Kang, H. M. Kim, Y. I. Park, T. Hyeon and D. H. Kim, *Adv. Mater.*, 2017, **29**, 1603169.
36 X. Wu, Y. Zhang, K. Takle, O. Bilsel, Z. Li, H. Lee, Z. Zhang, D. Li, W. Fan, C. Duan, E. M. Chan, C. Lois, Y. Xiang and G. Han, *ACS Nano*, 2016, **10**, 1060–1066.
37 D. Wang, D. Wang, A. Kuzmin, A. Pliss, W. Shao, J. Xia, J. Qu and P. N. Prasad, *Adv. Opt. Mater.*, 2018, **6**, 1701142.
38 B. Xue, D. Wang, L. P. Tu, D. P. Sun, P. T. Jing, Y. L. Chang, Y. L. Zhang, X. M. Liu, J. Zuo, J. Song, J. L. Qu, E. J. Meijer, H. Zhang and X. G. Kong, *J. Phys. Chem. Lett.*, 2018, **9**, 4625–4631.
39 D. Wang, B. Xue, X. G. Kong, L. P. Tu, X. M. Liu, Y. L. Zhang, Y. L. Chang, Y. S. Luo, H. Y. Zhao and H. Zhang, *Nanoscale*, 2015, **7**, 190–197.
40 F. Auzel, *Chem. Rev.*, 2004, **104**, 139–173.
41 D. Gao, X. Zhang, H. Zheng, W. Gao and E. He, *J. Alloys Compd.*, 2013, **554**, 395–399.
42 P. Salas, C. Angeles-Chavez, J. A. Montoya, E. De la Rosa, L. A. Diaz-Torres, H. Desirena, A. Martinez, M. A. Romero-Romo and J. Morales, *Opt. Mater.*, 2005, **27**, 1295–1300.
43 G. Chen, G. Somesfalean, Y. Liu, Z. Zhang, Q. Sun and F. Wang, *Phys. Rev. B: Condens. Matter Mater. Phys.*, 2007, **75**, 195204.
44 J. H. Zhang, Z. D. Hao, J. Li, X. Zhang, Y. S. Luo and G. H. Pan, *Light: Sci. Appl.*, 2015, **4**, e239.
45 D. Xu, C. Liu, J. Yan, S. Yang and Y. Zhang, *J. Phys. Chem. C*, 2015, **119**, 6852–6860.
46 R. B. Anderson, S. J. Smith, P. S. May and M. T. Berry, *J. Phys. Chem. Lett.*, 2014, **5**, 36–42.
47 F. Wang, Y. Han, C. S. Lim, Y. H. Lu, J. Wang, J. Xu, H. Y. Chen, C. Zhang, M. H. Hong and X. G. Liu, *Nature*, 2010, **463**, 1061–1065.
48 J. Zuo, L. P. Tu, Q. Q. Li, Y. S. Feng, I. Que, Y. L. Zhang, X. M. Liu, B. Xue, L. J. Cruz, Y. L. Chang, H. Zhang and X. G. Kong, *ACS Nano*, 2018, **12**, 3217–3225.
49 L. Wang, H. Dong, Y. N. Li, R. Liu, Y. F. Wang, H. K. Bisoyi, L. D. Sun, C. H. Yan and Q. Li, *Adv. Mater.*, 2015, **27**, 2065–2069.